Journal of Food Engineering 305 (2021) 110613

Contents lists available at ScienceDirect

Journal of Food Engineering

journal homepage: http://www.elsevier.com/locate/jfoodeng

Convective drying of highly shrinkable vegetables: New method on obtaining the parameters of the reaction engineering approach (REA) framework

Shilei Yang [a], Tao Liu [a], Nan Fu [a], Jie Xiao [a], Aditya Putranto [b], Xiao Dong Chen [a,*]

[a] Suzhou Key Laboratory of Green Chemical Engineering, School of Chemical and Environmental Engineering, College of Chemistry, Chemical Engineering and Materials Science, Soochow University, Suzhou, Jiangsu Province, 215123, PR China
[b] Discipline of Chemical Engineering, Monash University Malaysia, Bandar Sunway, Selangor, Malaysia

ARTICLE INFO

Keywords:
Reaction engineering approach
Convective drying
Dehydrated vegetable
Drying model
Shrinkage kinetics
Carrot

ABSTRACT

Accurate modeling of fruits and vegetables is difficult due to complications like non-regular shrinkage, wrinkling and skin formation. Comprehensively capturing these changes remain difficult. An interesting pathway through a rearranged set of heat and mass transfer equations to obtain the parameters for the drying kinetics model of the lumped reaction engineering approach (L-REA) is demonstrated. This approach allows the obtainment of REA parameters without worrying about shrinkage in the first place. Carrot, typical of a highly shrinkable vegetable, was dried at temperatures of 43, 55 and 63 °C and a fixed air velocity of 1.5 m/s. The REA parameters reveal a slightly lower additional activation energy compared with that from the classical approach. It can be seen that all moisture content and temperature profiles agree well with experimental data supported by R^2 higher than 0.9959 for moisture and 0.9837 for temperature which validates the proposed new approach is highly feasible for modeling of highly shrinkable vegetables. This work demonstrates the flexibility of the REA framework in avoiding interwinding issues with shrinkage data accuracy and the obtainment of REA parameters when testing highly shrinkable materials.

1. Introduction

Dehydration of fruits and vegetables is referred as an ordinary and economical way to lengthen preservation and increase added value. To date, the prosperous market of dehydrated commodities has spawned particular studies concentrating on dehydration process which gives fundamental guidance for promoting product quality and reducing energy consumption (Mahmutoglu et al., 1996; Mujumdar and Law, 2010; Li et al., 2019). In plenty of available studies, modeling the hygrothermal kinetics of foodstuffs offers a worthwhile path for the manufacture optimization (Defraeye and Radu, 2018).

Food materials especially the fruits and vegetables tend to shrink and fail to retain its original dimension when submitted to convective drying operation (Sander et al., 2001; Mayor and Sereno, 2004; Brasiello et al., 2017; Mahiuddin et al., 2018). Apart from the most evident change in decreased size, several sophisticated phenomena like wrinkling, crust formation and crack may concurrently occur owing to the nonuniform moisture distribution and multiphase constitution possessed by the specific variety of food matrix being processed (Mahiuddin et al., 2018; Singh and Talukdar, 2019). These morphological change is essential for supplementing detail to figure out the shrinkable area responsible for heat and mass transfer (Saha et al., 2018). Nevertheless, the complex and dynamic characteristics pertaining to highly shrinkable materials render the difficulty associated with precise measurement of transfer area is fiercely enhanced. Furthermore even under the most controlled drying conditions no food samples shrink and deform identically (Ortizgarciacarrasco et al., 2015). Despite the abundant experimental data on food shrinkage have been reported, how to implement the data for predictive purposes remains less convincing (Saha et al., 2018).

Empirical models are the most widely applied categories of drying model, which are established by simple or multivariable regression methods. While good for certain experimental situations, the empirical model may not be applicable to other conditions (Chen et al., 2001). For designing dryer and evaluation of dryer performance, effective and physically meaningful drying model should be implemented (Putranto and Chen, 2014). Reaction engineering approach (REA) is a

* Corresponding author.
E-mail address: xdchen@mail.suda.edu.cn (X.D. Chen).

https://doi.org/10.1016/j.jfoodeng.2021.110613
Received 8 November 2020; Received in revised form 8 March 2021; Accepted 29 March 2021
Available online 1 April 2021

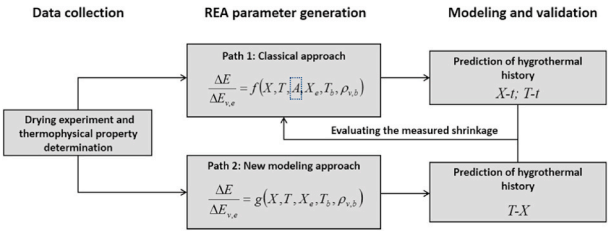

Fig. 1. Two paths for generating the REA parameter including the classical approach and new approach.

semi-empirical drying model to predict local or global hygrothermal evolution (Chen and Xie, 1997; Putranto and Chen, 2016a). It is a practical framework for establishing drying kinetics experimentally and theoretically. It is proved to be not only a new way of correlating the drying rate data, it also make the correlations more accurate and more sensible in terms of the physics involved (Chen, 2008). Evaporating surface area is included in the overall heat and mass balances that incorporate the classical REA to either generate the kinetic parameters of REA from experiments like the activation energy and the pre-exponential factor, or predict the temperature-time and the moisture-time profiles once REA is established. As such, having shrinkage data and model is necessary for generating the classical REA parameters. However, in the case where shrinkage is complex to quantify precisely, it is difficult to know if the REA parameters are affected by the shrinkage data. The REA parameters are supposed to reflect the moisture removal characteristics only, i.e. not affected by the accuracy of the shrinkage data. If we are able to isolate the effect of shrinkage from REA establishment we would be able to generate a 'clean' set of REA parameters. Then we can actually 'come back' to see if our shrinkage measurement is valid or not by comparing the predictions of temperature-time and moisture-time profiles obtained experimentally where the shrinkage data/model had to be used.

Due to the potential difficulty of classical approach when encountering highly shrinkable materials, a new approach to obtain the REA parameters without the need of measuring the changes of surface area during drying is proposed and exercised. Comparisons of this new approach with the classical approach (where the REA parameters are obtained through experiments involving the measurement of surface area) are undertaken. The objective of current work is to verify the predictive availability of this new approach and develop an alternative modeling path of REA framework to simulate highly shrinkable materials.

2. Theoretical background

2.1. The classical REA

The main differences between the two pathways for yielding the REA parameter, one classical and one new, are indicated in Fig. 1. More precisely, we are talking about the lumped REA here, i.e. L-REA. Without any assumption, the mass balance around the object being dried can be formulated as (Chen, 2008):

$$m_s \frac{dX}{dt} = -h_m A(\rho_{v,s} - \rho_{v,b}) \tag{1}$$

where m_s is dry basis mass (kg), t is drying time (s), X is moisture content (kg·kg^{-1}, on dry basis), $\rho_{v,s}$ and $\rho_{v,b}$ refer to the vapor concentration at material surface and at the drying medium (kg·m^{-3}), h_m represents the mass transfer coefficient (m·s^{-1}) and A is the surface area responsible for heat and mass transfer (m^2). Generally, mass transfer coefficient (h_m) may be calculated from the established Sherwood number correlations or experimentally measured for practical scenarios (Patel et al., 2009). Surface vapor concentration ($\rho_{v,s}$) varies constantly with sample

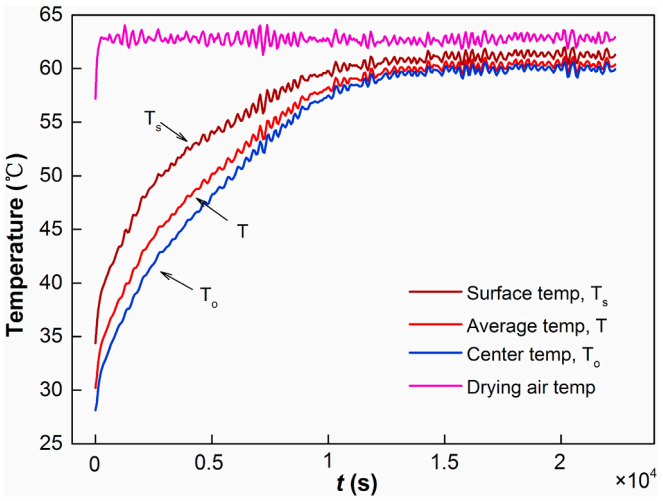

Fig. 2. Temperature difference within the carrot cube dried at 63 °C.Average temperature here was computed according to Eq. (A-3) in Appendix while surface and center temperature were extracted from the experimental data.

temperature, which can be correlated with the saturated vapor concentration ($\rho_{v,sat}$) as follows (Chen, 2008):

$$\rho_{v,s} = \exp\left(\frac{-\Delta E_v}{RT}\right)\rho_{v,sat}(T) \tag{2}$$

where $\triangle E_v$ refers to the additional activation energy to remove moisture from the material beyond the free water effect (J·mol^{-1}) and is ideally considered to be moisture content (X) dependent only (Chen et al., 2001). R is the universal gas constant (8314 J mol^{-1}·K^{-1}). T is the sample mean temperature (K) for L-REA. Here essentially, evaporation is regarded as an activation process in the REA framework.

For small objects like droplet or thin layer material, or even larger materials of a few mm, the mean temperature may be justified as approximately the surface temperature anyway, which may be validated using the Chen-Biot number analysis (Chen and Lin, 2005).

As the carrot sample investigated was having a considerable initial size (in the order of cm), the temperature within the sample could not be regarded as uniform as shown in Fig. 2. For employing the L-REA, a parabolic temperature distribution has been adopted which has been shown satisfactory before (see Appendix) (Chen and Xie, 1997; Putranto et al., 2011).

It is highlighted that all subsequent temperatures used for calculation and representation are the average values of the entire carrot sample. Saturated vapor concentration of water ($\rho_{v,sat}$) can be estimated using the following equation:

$$\begin{aligned}\rho_{v,sat} = {} & 4.844\times10^{-9}(T-273)^4 - 1.4807\times10^{-7}(T-273)^3 + 2.6572 \\ & \times10^{-5}(T-273)^2 - 4.8613\times10^{-5}(T-273) + 8.342\times10^{-3}\end{aligned} \tag{3}$$

which is based on the literature data (273.15 K–430 K) (Keey, 1992).

The mass balance (Eq. (1)) can be combined with Eq. (2) and expressed in the following form:

$$m_s \frac{dX}{dt} = -h_m A\left[\exp\left(\frac{-\Delta E_v}{RT}\right)\rho_{v,sat}(T) - \rho_{v,b}\right] \tag{4}$$

The apparent activation energy ($\triangle E_v$) is the fundamental parameter of REA modeling and can be determined experimentally with variables (dX/dt, T and A) (Compaore et al., 2017). By rearranging Eq. (4), the $\triangle E_v$ is accordingly written as follows:

Table 1
Experimental conditions during convective drying of carrot cubes.

Air flow conditions	Temperature	43 ± 0.5 °C	55 ± 0.5 °C	63 ± 0.5 °C
	Velocity		1.5 m/s	
	Relative humidity	2.66 ± 0.32%	7.2 ± 0.51%	0.51 ± 0.04%
Carrot parameters	Initial moisture content		11.09 ± 0.43 kg/kg	
	Initial size		1 × 1 × 1 cm^3	
			0.22 kg/kg	0.10 kg/kg
	Equilibrium moisture content	0.44 kg/kg		

$$\Delta E_v = -RT \ln\left[\frac{-m_s \frac{dX}{dt}\frac{1}{h_m A} + \rho_{v,b}}{\rho_{v,sat}(T)}\right] \tag{5}$$

The apparent activation energy during a drying process can be normalized with the equilibrium or maximum activation energy $\triangle E_{v,e}$, in the form of $\triangle E_v/\triangle E_{v,e}$ (0-1 scale). Previous studies have shown this normalized activation energy $\triangle E_v/\triangle E_{v,e}$ can be correlated to the reduced moisture content $X–X_e$ of material being dried using an empirical function (Patel et al., 2009; Fu et al., 2012).

$$\frac{\Delta E_v}{\Delta E_{v,e}} = g(X - X_e) \tag{6}$$

where g is the function describing the best correlation, X_e is the equilibrium moisture content (kg.kg^{-1}, on dry basis). When the surface vapor density $\rho_{v,s}$ achieves equilibrium with the bulk air vapor density $\rho_{v,b}$, drying ceases due to no more driving force. At this stage, the apparent activation energy $\triangle E_v$ achieves maximum, i.e., $\triangle E_{v,e}$ (Patel et al., 2009; Fu et al., 2012):

$$\Delta E_{v,e} = -RT_b \ln(RH_b) \tag{7}$$

where RH_b (=$\rho_{v,b}/\rho_{v,sat}$ (T_b)) and T_b refer to the relative humidity and temperature of drying air, i.e. bulk properties, respectively. The details of air flow condition and moist sample parameter are listed in Table 1.

It is further noted that with the aim to cover the 'whole range' of the moisture content, i.e. to have the activation energy for the material at any stage of dryness, experiments are preferred to carried out with rather dry air (with known humidity nevertheless) (Putranto and Chen, 2013, 2016b).

Since the thermal energy transferred to the moist material is used for both latent and sensible heating, the heat balance is deduced as follows provided other volatile components are negligible (Kharaghani et al., 2019):

$$mC_p\frac{dT}{dt} = hA(T_b - T) + \Delta H_v m_s \frac{dX}{dt} \tag{8}$$

where m is the sample mass (kg), C_p is specific heat capacity of the sample (J·kg^{-1}·K^{-1}), h is the heat transfer coefficient (W·m^{-2}·K^{-1}) and $\triangle H_v$ represents the latent heat of water vaporization (J·kg^{-1}). Notice that the premise of Eq. (8) is a representative mean temperature to allow the heat balance in a lumped mode for the sample being dried.

2.2. Gaining REA parameters independent of the shrinkage data

To achieve the above-mentioned strategy to isolate shrinkage data requirement, some considerations of the heat and mass balance equations are necessary. The mass and specific heat capacity in Eq. (8) may be expressed as the following:

$$m = m_s(1 + X) \tag{9}$$

$$C_p = C_{p,s}\frac{1}{(1+X)} + C_{p,w}\frac{X}{(1+X)} \tag{10}$$

where $C_{p,s}$ and $C_{p,w}$ are the specific heat capacity of dry mass and water, respectively, (J·kg^{-1}·K^{-1}). Subsequently, heat balance (Eq. (8)) can be rewritten as:

$$m_s(1+X)\left[C_{p,w}\frac{X}{(1+X)} + C_{p,s}\frac{1}{(1+X)}\right]\frac{dT}{dt} = hA(T_b - T) + \Delta H_v m_s \frac{dX}{dt} \tag{11}$$

Both sides of the above equation are divided with the rate of moisture loss, (i.e. using Eq. (4)). The following expression can be obtained:

$$\left(C_{p,w}X + C_{p,s}\right)\frac{dT}{dX} = -\left(\frac{h}{h_m}\right)\frac{(T_b - T)}{\exp\left(\frac{-\Delta E_v}{RT}\right)\rho_{v,sat}(T) - \rho_{v,b}} + \Delta H_v \tag{12}$$

where dT/dX represents the ratio of moisture content and temperature at corresponding time. After rearranging Eq. (12), the apparent activation energy ($\triangle E_v$) can be obtained through the following equation:

$$\Delta E_v = -RT \ln\left\{\frac{\left[\frac{\left(C_{p,w}X + C_{p,s}\right)\frac{dT}{dX} - \Delta H_v}{-\left(\frac{h}{h_m}\right)(T_b - T)}\right]^{-1} + \rho_{v,b}}{\rho_{v,sat}(T)}\right\} \tag{13}$$

It is appeared that as long as the moisture content versus time and temperature versus time data can be reliably obtained, one can work out the $\triangle E_v$. This is in a good contrast with the classical approach (Eq. (5)). Here the surface area effect, the same as said for shrinkage, is removed to obtain the activation energy.

Table 2
Thermodynamic properties of drying air (Chen and Xie, 1997; Patel et al., 2009).

Physical and thermodynamic properties	Calculation
Heat capacity (J·kg^{-1}·K^{-1})	1.9327 × 10-10T^4 -7.999 × 10-7T^3 +1.1407 × 10-3T^2 -0.4489 T + 1057.3 (295 K < T < 800 K, R^2 = 0.9995)
Thermal conductivity (W·m^{-1}·K^{-1})	0.0000778 T + 0.00274 (250 K < T < 400 K, R^2 = 0.9996)
Density (kg·m^{-3})	(273.15 × 1.2928)/T
Viscosity (Pa·s^{-1})	1.691 × 10^{-5} +4.984 × 10^{-8} T -3.187 × 10^{-11}T^2 +1.319 × 10^{-14}T^3 (250 K < T < 400 K, R^2 = 0.9996)
Vapor-air diffusivity (m^2·s^{-1})	1.963 × 10^{-7} T -3.33307 × 10^{-5} (293 K < T < 373 K, R^2 = 1.0)
Latent heat of water vaporization (J·kg^{-1})	3,158,100–2401.8 T (290 K < T < 370 K, R^2 = 0.9997)

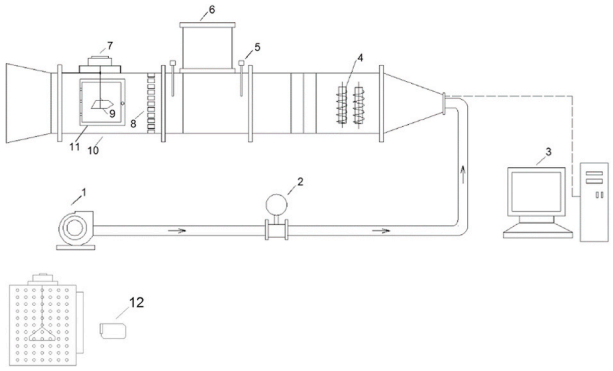

Fig. 3. Schematic illustration of drying system. 1. Air blower; 2. Turbine flow meter; 3. Control computer; 4. Heating element; 5. Thermocouple; 6. Switchable bypass; 7. Digital balance; 8. Metal grid; 9. Loaded tray; 10. Drying chamber; 11. Observation window; 12. Video camera.

2.3. Heat and mass transfer coefficients

In the new approach, one still needs the transfer coefficients, at least the ratio of them. The mass transfer coefficient, h_m and heat transfer coefficient, h of this study were determined from the established Sherwood number (*Sh*) and Nusselt number (*Nu*) for evaporating pure water under a series of known environmental conditions (Ranz and Marshall, 1952; Chen and Xie, 1997). The relevant *Reynolds* number was corrected by referring to the literature (Pasternak and Gauvin, 1960) for considering the scenario of cubic sample and the face parallel to air stream. The established Sherwood and Nusselt correlations are given as follows:

$$Sh = \frac{h_m L}{D_f} = 0.61(\mathrm{Re})^{1/2}(Sc)^{1/3} \tag{14}$$

$$Nu = \frac{hL}{k_f} = 0.613(\mathrm{Re})^{1/2}(\mathrm{Pr})^{1/3} \tag{15}$$

where L is the length (size) of sample (m), D_f refers to the vapor-in-air diffusion coefficient (m^2. s^{-1}) and k_f is thermal conductivity of drying air ($W{\cdot}m^{-1}{\cdot}K^{-1}$) at film temperature denoted with f (the average of the sample temperature and the gas temperature). *Re*, *Sc* and Pr are the *Reynolds*, *Schmidt* and *Prandtl* numbers, respectively. Calculating formulas about required drying gas physical properties for estimating h, h_m and other thermodynamic properties for REA simulation are listed in Table 2. Several similar drying cases have been investigated in literatures to probe the mass and energy transfer which take place in carrot drying (Suzuki et al., 1977; Mulet et al., 1989).

The appropriate type of convection transfer coefficient is associated with the object geometry according to the literature reported by Incropera and Dewitt (1985). For the heat and mass transfer scenarios like flat plate and cylinder and parallel flow, the correlation used like here is basically valid instead of using a general type equation for a single droplet or sphere. Consequently, this makes it convenient to straightforwardly harvest the ratio of heat to mass transfer coefficient and as a result, it is surprising to notice that shrinking effect totally disappears in new approach. The ratio of heat to mass transfer coefficient would involve drying gas properties only as:

$$\frac{h}{h_m} = \frac{k_f}{D_f}\left(\frac{D_f}{k_f} C_{p,f}\rho_f\right)^{1/3} \tag{16}$$

where $C_{p,f}$ and ρ_f is the specific heat capacity ($J{\cdot}kg^{-1}{\cdot}K^{-1}$) and density ($kg{\cdot}m^{-3}$) of drying air at film temperature.

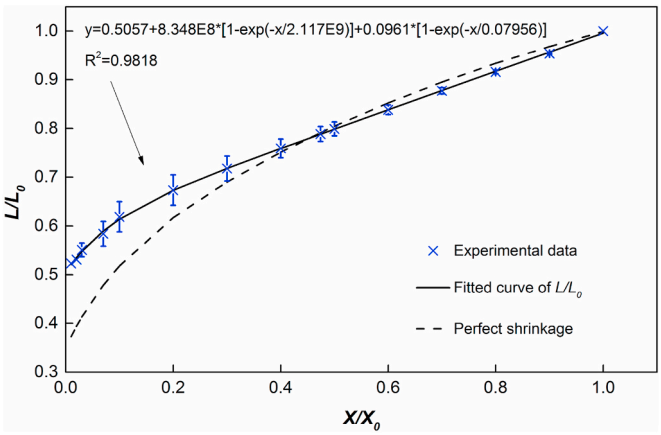

Fig. 4. Shrinkage kinetics of side lengths of carrot cube at experimental conditions.

3. Material and methods

3.1. Materials

Raw carrots (*Daucus carrota* L.) were procured from a local market in Suzhou, China. They were selected with similar sizes, color and without visible damages, then stored in a refrigerator (4 °C, 95% RH) until used. Before experiments, carrot was warmed up to room temperature, washed, peeled and diced into 1 cm × 1 cm × 1 cm cubes with a customized steel mould. Initial mass discrepancy among all used samples was controlled within 0.05 g. The initial moisture content of carrot was gravimetrically determined to be 11.09 ± 0.43 kg kg^{-1} (on dry basis) by the oven method 935.29 (AOAC, 1995).

3.2. Experimental procedure

The convective drier used in this work was a single-sample unit (Nantong Dong Concept New Material Technology, Nantong, China). A schematic figure of the drier set-up is shown in Fig. 3. Briefly, there was a blower (XBH-370, TIANZELU, TIANTAI MACHINERY CO., LTD, China) supplying airflow into the drying system. The drying air stream was subsequently heated to the desired temperature and was passed through a metal meshes with evenly spaced circular holes setting at the entrance of the chamber in order to achieve a laminar parallel flow within the drying chamber. The cross-sectional area of the drying chamber was 95 × 95 mm which was much larger than that of the carrot sample. Both the inlet and outlet of chamber were attached with K-type thermocouples to monitor and assure a stable state prior to experiments. A digital balance (PX 225DZH, OHAUS, USA, precision 0.1 mg) was positioned just above the drying chamber and linked to the tray with a thin wire. The relative humidity of the air stream was recorded by using relative humidity data logger (500 B, KAIXIANG Instruments Co., China).

Drying was performed at three different conditions shown as Table 1. The air velocity was constant at 1.5 m s^{-1}. When transferring a carrot sample into the drying chamber, a bypass barrier plate was used to divert the conditioned hot air stream away, thus minimizing evaporation before monitoring began. The dimension, temperature and mass data of the carrot during drying were obtained in parallel runs with identical experimental condition. Drying proceeded until the carrot mass remained essentially constant at least for 30 min.

Temperature measurement was carried out with inserted thermocouples (K type, CHAL001, Omega Engineering, USA, precision 0.01 °C) at the geometrical center, windward and leeward and side surface of carrot cube (fixed depth: 5 mm at center; 1 mm at surface). The temperature data were obtained from data logger (Picolog R5.17, Pico

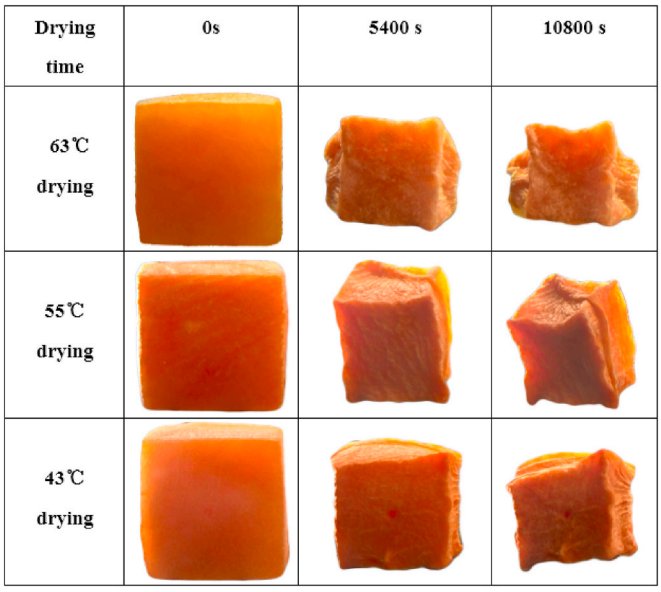

Fig. 5. Morphological image of carrot cube.

Technology, UK) at 60 s time interval. Endothermic influence of thermal sensors was omitted. Temperatures at carrot surface were averaged as a unified superficial value to minimize the error caused by air stream and further used to estimate transfer coefficient. It is worth noting that the temperature of carrot would reach a relative equilibrium state preceded by that of moisture content in all drying cases.

Mass measurement and dimension recording are carried out meantime. The mass readings from digital balance were consecutively transmitted to the computer. The whole drying process was recorded using a video camera (HDR-CX405, SONY, Japan) at 10–20 times magnification. This camera can provide a resolution of approximately 9.2 megapixels. A LED light source on the opposite side of the drying chamber was placed to keep the drying chamber bright and guarantee the high-quality captured images. The first image was captured immediately after placing the carrot cube in the drying chamber. From then onwards, images were captured at 10-min interval. For image analysis purpose, raw images were converted to TIF format and cropped to a size of 850 × 800 pixels only including the carrot sample. The sequence of images was analyzed with the ImageJ 1.40f (National Institutes of Health, Bethesda, MD, USA) to estimate the shrinking size. As the magnification of camera lens stayed the same in one drying run, a calibration factor was established by counting the pixels in a known distance in the initial side length of prepared carrot cube. The scale of the images was 75 pixels/mm. It was hypothesized that carrot cube kept square for entire drying duration. Owing to the shrinkage complication in late drying period, the variation of side length was chosen to represent the shrinking process. Fig. 4 displays the evolution of side lengths with respect to the moisture content. The morphological images of carrot cube are shown in Fig. 5. A similar method was earlier employed to analyze droplet shrinkage behavior and the resultant REA parameters could be satisfactorily obtained (Fu et al., 2011, 2013; Haque et al., 2016).

3.3. Regression appraisal

The fitness of normalized activation energy as well as the modeling performance of new method and classical method of REA for simulating the drying of highly shrinkable carrot was evaluated using statistical parameters such as coefficient of correlation (R^2) and the root mean square error (*RMSE*):

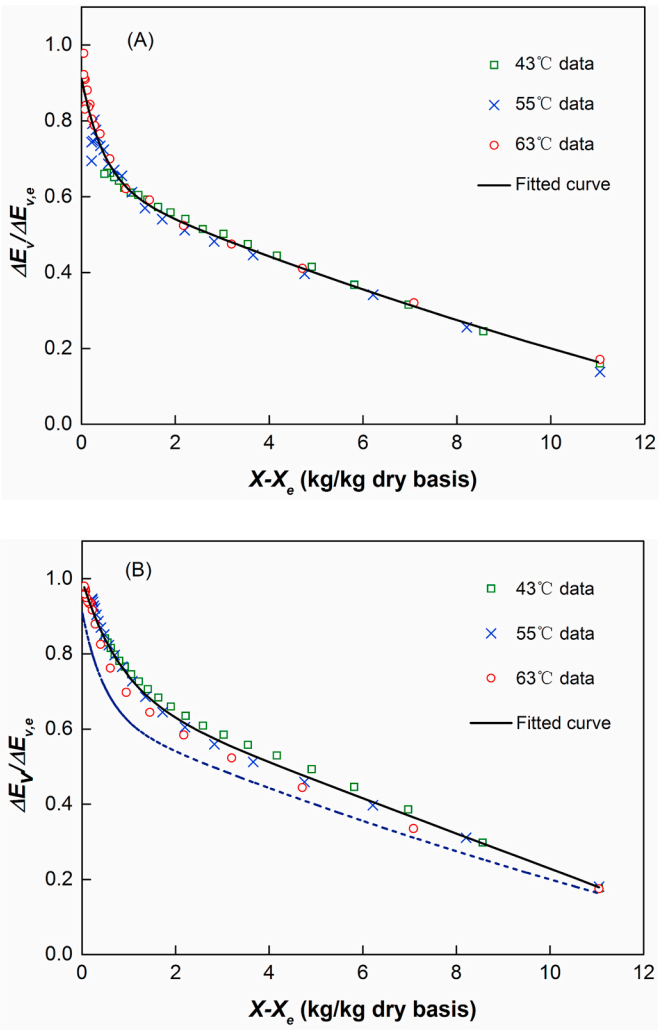

Fig. 6. Relative activation energy plotted against moisture content at experimental conditions and the fitted normalized activation energy curve: A) new modeling approach; B) classical modeling approach. The normalized activation energy by new approach is represented as dashed line for comparison.

$$R^2 = 1 - \left(\frac{\sum_{i=1}^{N} \left(Y_{\exp,i} - Y_{pre,i}\right)^2}{\sum_{i=1}^{N} \left(Y_{\exp,i} - Y_{mean}\right)^2} \right) \tag{17}$$

$$RMSE = \left[\frac{1}{N} \sum_{i=1}^{N} \left(Y_{pre,i} - Y_{\exp,i}\right)^2 \right]^{1/2} \tag{18}$$

where $Y_{\exp,i}$ is the experimental data of the investigated variable, Y_{mean} is the average value of experimental data, $Y_{pre,i}$ is the predicted value using REA modeling, N is the number of observations.

Table 3
Constants in fitted functions (Eq. (19)) of normalized activation energy.

	New approach	Classical approach
Coefficient A_1	0.2752	0.3243
Coefficient A_2	−0.4747	−0.9332
Coefficient B_1	1.3822	2.8564
Coefficient B_2	−26.2172	−52.3376
Coefficient C_1	−0.7438	−2.1726
R^2	0.9790	0.9913
RMSE	0.0221	0.0189

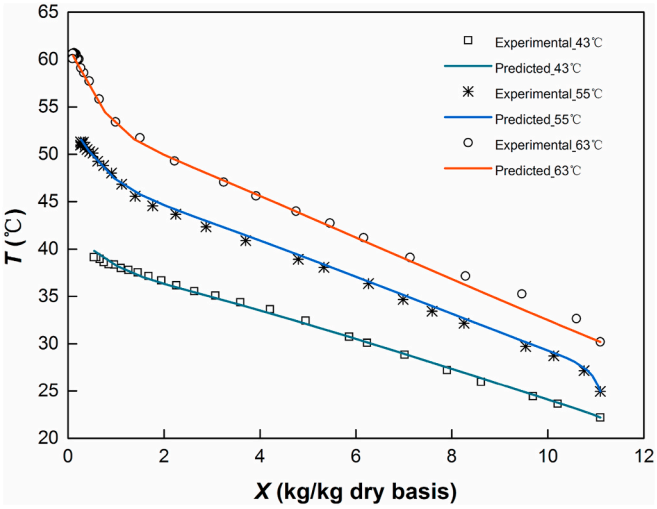

Fig. 7. Modeling result using new approach (lines) vs. experimental data (symbols) at three experimental conditions.

4. Results and discussion

4.1. Generation of activation energy

The unique relative activation energy ($\triangle E_v/\triangle E_{v,e}$) of carrot should be yielded in priority to simulate the hygrothermal behavior at experimental conditions using L-REA. On the basis of reliable experimental drying data, the relative activation energy is calculated and correlated towards the moisture difference (X–X_e) as exhibited in Fig. 6A and B. It appears that the plots of relative activation energy under different drying environments seem independent of drying conditions and follow a similar trend. This consequence is in line with previous studies in which the modification of drying conditions does not affect much the REA parameters as surely that the REA parameters represent the moisture removal phenomena of the material constituents (Chen and Xie, 1997; Patel et al., 2009; Putranto and Chen, 2014).

Afterwards one fitted normalized activation energy can be obtained by least square method using Eq. (19). It is indicated in Fig. 6A and B that the fitted normalized activation energy curve matches the experimental relative activation energies. The relationship between the normalized activation energy and the moisture difference from both L-REA approaches can be appropriately correlated using the following equation:

$$\frac{\Delta E_v}{\Delta E_{v,e}} = A_1 \exp\left(\frac{X - X_e}{A_2}\right) + B_1 \exp\left(\frac{X - X_e}{B_2}\right) + C_1 \tag{19}$$

where A_1, A_2, B_1, B_2 and C_1 are the matched constants and their values are listed in Table 3. This particular formula has not been used before as the activation energy expression.

On the whole the relative activation energies ($\triangle E_v/\triangle E_{v,e}$) from two L-REA approaches are pretty similar in trending against water content difference. The curves for 43, 55, 63 °C respectively can be seen to approach each other which shows the $\triangle E_v/\triangle E_{v,e}$ responding to evaporation is mostly an inherent material property (Chen, 2008). It is not necessary to refit the empirical function $g(X–X_e)$ when the drying surrounding is altered provided the same material with similar initial moisture content. That is to say only one accurate drying experiment is needed to yield data for generating REA parameters (Putranto and Chen, 2016b). The curve obtained by employing the new approach (in Fig. 6A) is slightly lower (refer to the dashed line shown in Fig. 6B). When approaching the final state, the activation energy curves all go up more dramatically. Initial values of $\triangle E_v/\triangle E_{v,e}$ in both Fig. 6A and B appear to be above zero, implying the carrot surface was not 'fully covered' with free water as such. The curve reflects mainly the impact of the interior structure on the sample being dried.

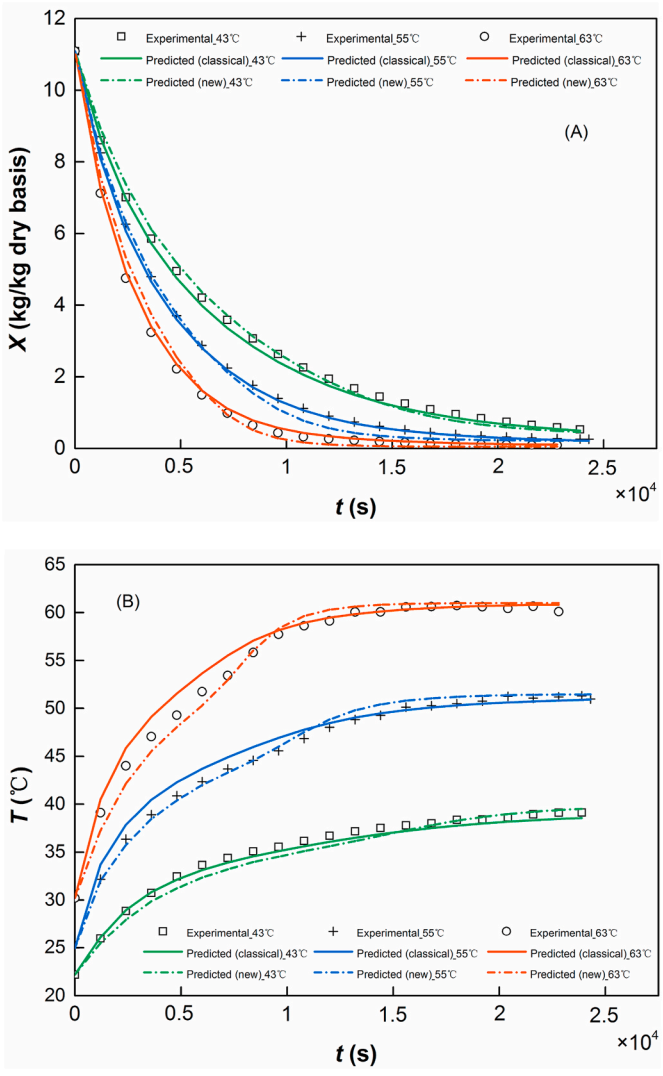

Fig. 8. Modelled profiles with respect to drying time using classical approach (lines) and new approach (dash dot lines) vs. experimental data (symbols) at three experimental conditions. (A) Moisture content; (B) temperature.

For acquiring both modeling profiles of moisture content and temperature of convective drying of carrot cube using the two L-REA approaches, respectively, the mass and heat balance (Eqs. (4) and (8)) or the comprehensive heat and mass balance (Eq. (12)) are solved simultaneously in conjunction with respective normalized activation energy (Eq. (19)) and equilibrium activation energy (Eq. (7)) using ordinary differential equation solver *ode23s* available in software Matlab® (Mathworks Inc., 2018).

4.2. Validation of the new approach for L-REA

The L-REA parameters obtained through the new pathway are used to model the convective drying of highly shrinkable carrot cubes at drying air temperature of 43, 55, 63 °C.The relationship between moisture content and corresponding temperature is shown for each drying condition. The relationship is different from that for the onion and kiwifruit pulp (Chen et al., 2001; Compaore et al., 2017). Excellent agreement between the predicted and experimental data of the mean temperature versus the moisture content is shown in Fig. 7, with correlation coefficient $R^2 = 0.9954$ for 43 °C, $= 0.9981$ for 55 °C, $= 0.9903$

Table 4
Statistical analysis for the REA modeling.

	Drying temp (°C)	R^2 for X	*RMSE* for X	R^2 for T	*RMSE* for T
New approach	43	0.9990	0.1819	0.9837	0.8382
	55	0.9984	0.1842	0.9975	0.5802
	63	0.9959	0.2511	0.995	1.1748
Classical approach	43	0.9991	0.1526	0.9978	0.4805
	55	0.9998	0.0779	0.9906	0.9770
	63	0.9996	0.1012	0.9895	1.0645

for 63 °C respectively. There is a slight underestimation of predicted temperature in the early period of 63°Cdrying which may be due to the sensitivity of activation energy fitting in this part of the trend.

This new approach exhibits the capability to obtain L-REA parameters without the need to know prior the surface area of the sample during drying. Of course, in order to predict the temperature-time and moisture content-time profile, one has to know the surface area. This new approach has allowed the obtainment of the REA parameters independent of the data on surface area. In other words the REA parameters as obtained are not affected by the potential errors in surface area measurement in the first place.

4.3. Assessment of the classical approach for L-REA

Results of the classical approach for modeling convective drying of the carrot cubes are revealed in Fig. 8A and B. In Fig. 8A, the predicted moisture content versus time is benchmarked against the experimental data and good agreement is observed ($R^2 = 0.9991$ for 43 °C, = 0.9998 for 55 °C, = 0.9996 for 63 °C respectively). It can be found that the modelled temperature versus time shown in Fig. 8B match well with the experimental data ($R^2 = 0.9978$ for 43 °C, = 0.9906 for 55 °C, = 0.9895 for 63 °C, respectively). The values of statistical parameters are sufficient to justify the goodness of fit of the model, showing the reaction engineering approach (REA) can represent both moisture content and temperature well during drying (Kucuk et al., 2014). Similar good

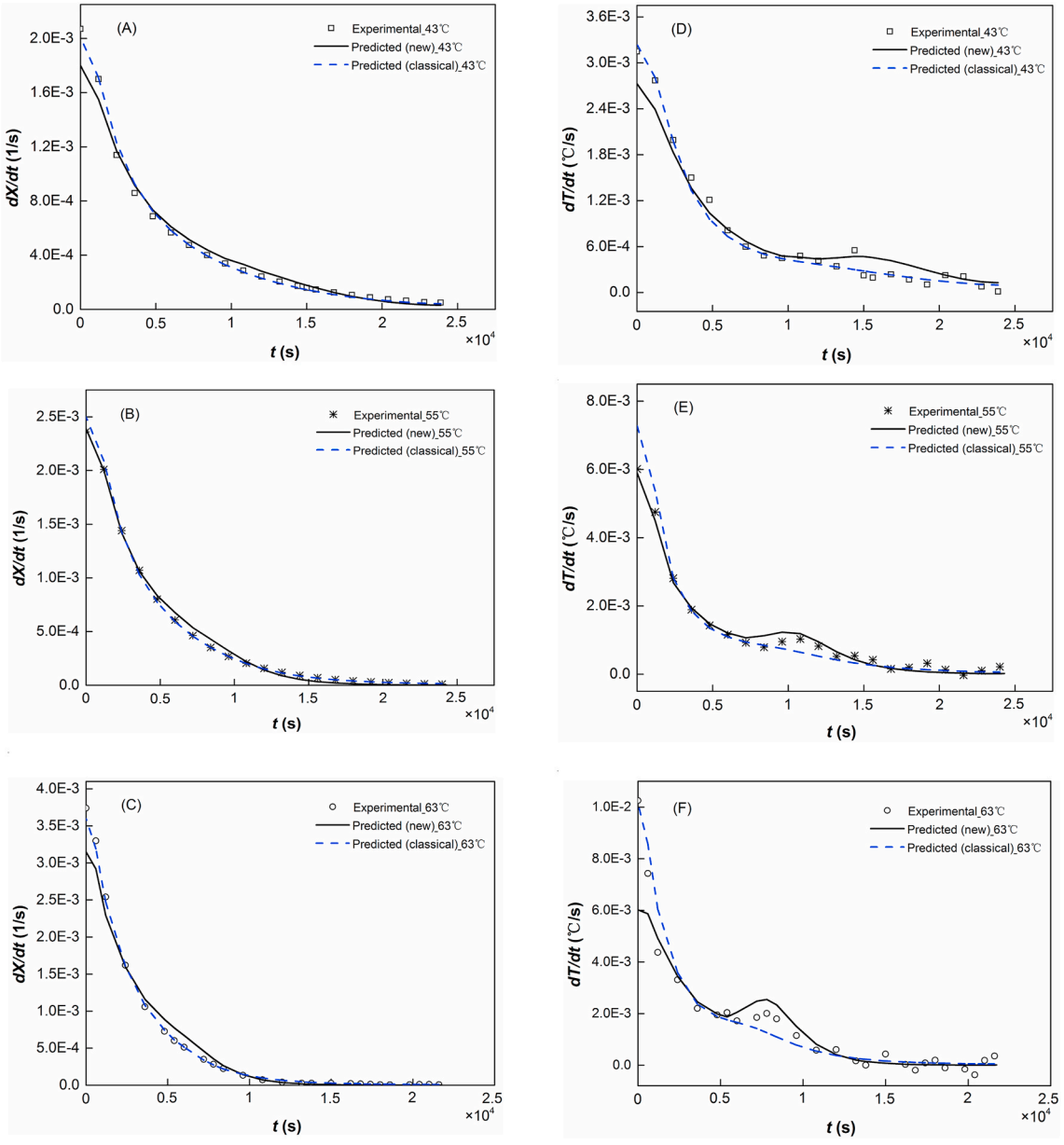

Fig. 9. Comparison of the experimental variation rate in moisture removal and temperature and the predictions given by the two L-REA approaches. (A–C) Moisture removal rate; (D–F) temperature change rate.

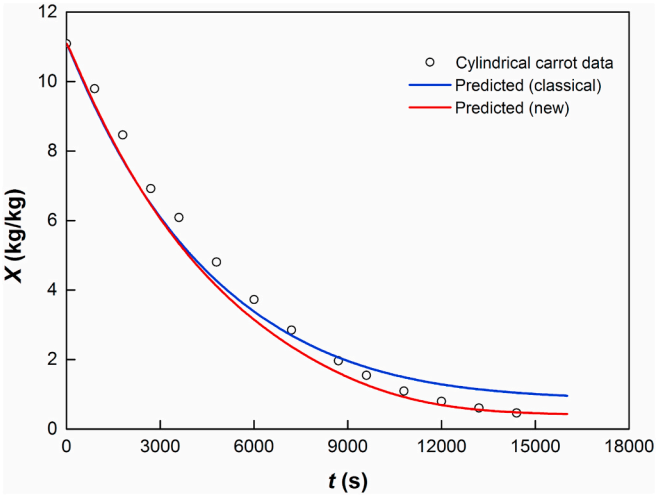

Fig. 10. Predicted moisture profile of carrot cylinder (diameter: 2.15 cm; height: 0.48 cm; X_0 = 11.20 kg/kg) dried at 70 °C, 0.35 m/s.

performances are shown in REA modeling of the drying of mango and apple tissues (Putranto et al., 2011). On the other hand, combining the already verified REA parameters of new approach and the measured shrinkage data can create the hydrothermal simulation with time reference, which are profiled in Fig. 8A and B as well. Satisfactory agreement can be observed and the correlation coefficient R^2 is listed in Table 4. It can be reasonably inferred at least for this case, i.e. the carrot drying, that the shrinkage data obtained from photographic technique is applicable enough to yield an acceptable simulation using the both approaches.

However for the photographic technique, a limitation of this method should be pointed out that only one surface can be photographed and assuming perfect cube, one could estimate the shrinkage. After modeling the drying behavior of carrot cube with ideal shrinkage model (shown in Fig. 4) with the new REA approach, it is found that the ideal shrinkage data can already provide a slightly closer agreement with experiments than the measured shrinkage data from the image analysis. It can be deduced that the change of surface area may be closer to the ideal shrinkage. It is an advantage of the new approach of L-REA is that the REA parameters can be obtained independent of the surface area. Then the shrinkage model can be evaluated consequently.

4.4. Drying rate and rate of temperature change

As shown in Fig. 9A–F, the moisture removal rate together with the rate of temperature change of carrot cubes dried at different convective drying conditions are plotted with respect to time. It can be seen that the predicted results obtained from both L-REA approaches can match well with the experimental data. The endpoint of convective drying operation of carrot seems to be well projected using the L-REA approaches which can provide guidance for practical situation. The experimental temperature rate curves are observed to oscillate after drying for a period of time and part of the oscillations are reflected by the new method (Fig. 9D–F). From Fig. 2, the measurements of temperature are known to have sensor noise. We attempt to remove the noise by sampling sensor data at drying times (here at a 20-min interval) which is a required step both to produce the plot of average temperature versus moisture content shown in Fig. 7 and to smooth out errors during the numerical differentiation of experimental temperature data, as very small differences in temperature values over a short time interval could potentially lead to enormous changes in dT/dt or dT/dX values, resulting from data structure rather than a real behavior.

Two kinds of 'oscillations' are exhibited in Fig. 9D–F. The initial experimental 'humps' about 0.8E4 to 1.5E4 s are part of the real

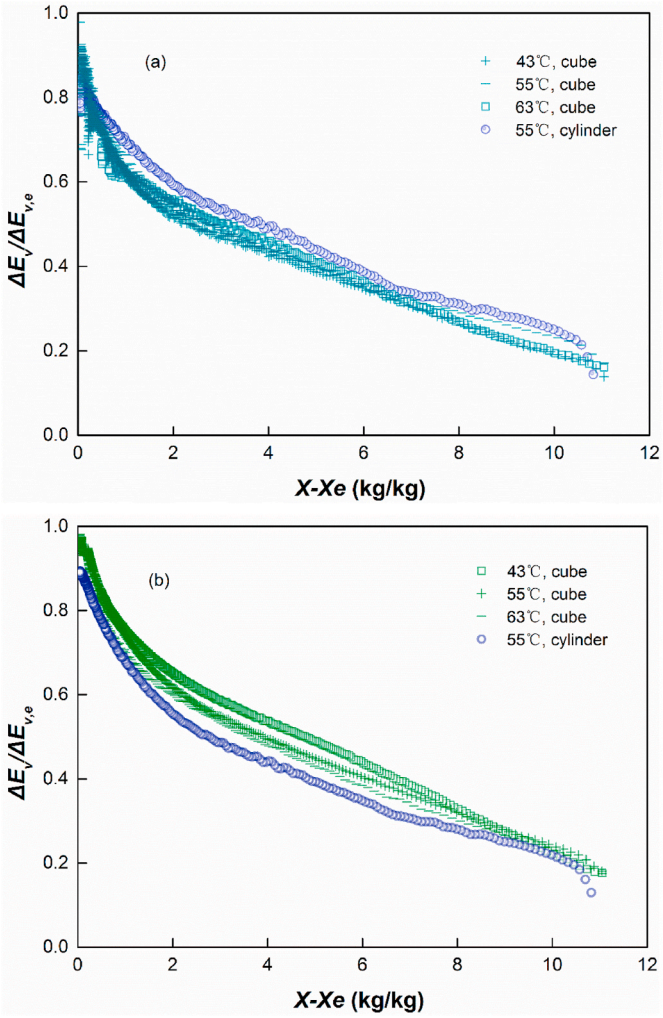

Fig. 11. Relative activation energies of cubic carrot (43, 55 and 63 °C, 1.5 m/s) and cylindrical carrot (55 °C, 1.5 m/s) using (a) new method and (b) classical method.

experimental behavior, not caused by measurement errors, as they coincide with inflexions in plots of T versus X (Fig. 7) at about 1 kg water/kg solid and in heating curves (Fig. 8; here the effect is subtle but may have been amplified by the numerical differentiation). This behavior is properly captured by the inflexion of relative activation energy in Fig. 6A at about 1 kg water/kg solid, leading to 'humps' in Fig. 9. Therefore, these 'humps' do not result from model inadequacy or overfitting as in polynomial functions. On the other hand, final experimental 'oscillations' when dT/dt approaches zero do result from experimental records. This behavior is however correctly 'discarded' by the model because the relative activation energy (Fig. 6A) does not exhibit further changes in its trend at corresponding moisture contents. It is worth noting that the selected time interval here is to make an intuitively correct rate profile, not for deliberately fitting or smoothing the experimental curve.

4.5. Modeling of cylindrical carrot

In order to further show the implemented new method which is less influenced by the surface state, another geometry of carrot, i.e. cylindrical carrot sample (diameter: 2.15 cm, height: 0.48 cm), was experimented. Then the simulation was carried out with the normalized activation energy of 1 cm carrot cube (Eq. (19)). The modeling outcome using new method in Fig. 10 shows better agreement with experimental

results. The highly possible reason is the similar trends of relative activation energy using new approach of cylindrical carrot with that of carrot cube. Fig. 11a and b clearly plot the difference of relative activation energy. It is indicated in Fig. 11a that the difference is not obvious as surface state is circumvented in new method which makes it reasonable to use the relative activation energy from one drying experiment to extrapolate the drying kinetics under other conditions. It can be seen in Fig. 11b that minor difference exists when using classical method because surface state is involved in generating the REA parameter and hence the resultant relative activation energy may differ. We have also experimented and simulated the carrot cube with different initial dimensions. The simulation was also satisfactory. Fu et al. (2011) found the similar results for the drying of droplets with different initial droplet sizes.

5. Conclusion

In this study, the REA-based drying kinetics models are formulated for the convective drying of a highly shrinkable vegetable, i.e. carrot cubes. For the first time, a new modeling method is found to allow the obtainment of the REA parameters without worrying about the shrinkage which eliminates the potential interference due to the incorporation of shrinkage information which is difficult to measure in generating activation energy. When benchmarked against the experimental data, both REA methods are accurate for carrot cubes anyway to capture the drying behaviors which is evidenced by the R^2 higher than 0.9837 for moisture content and temperature. This implies that the shrinkage measurement used in current approach is good enough for carrot cubes. For a material like leafy products, imaging may not be sufficient in gaining accurate shrinkage values.

The new method is effective but still needs good shrinkage data to predict time responses of temp and moisture. However this new method allows an independent evaluation on whether the shrinkage data was reliable or not when predicting experimentally measured temp-time, moisture-time relationships. The results show a great promise. This independence of shrinkage data may enable future modeling of temp-time and moisture-time profiles for process control purposes with a theoretically hypothesized shrinkage model, thus doing away the need for precise measurement of shrinkage which for vegetables and fruits is difficult to measure. This work will be reported in near future.

Credit author statement rev

Shilei Yang: experimental work, methodology, modelling, original manuscript writing. **Tao Liu**: experimental work, methodology, modelling, original manuscript writing. **Nan Fu:** conceptualisation, supervision, manuscript editing. **Jie Xiao:** conceptualisation, supervision. **Aditya Putranto:** conceptualisation, manuscript checking. **Xiao Dong Chen:** generation of ideas, conceptualisation, supervision, manuscript checking.

Declaration of competing interest

We declare that there is no conflict of interest among us for this paper. All authors are agreeable to submit our works to Journal of Food Engineering. We hope that this paper can be reviewed favourably.

Acknowledgement

This work was supported by National Key Research and Development Program of China (Project number 2017YFD0400905).

Nomenclature

a_w	Water activity
A	Surface area of sample, m^2
C_p	Specific heat of material being dried, $J{\cdot}kg^{-1}{\cdot}K^{-1}$
$C_{p,s}$	Specific heat of dry mass, $J{\cdot}kg^{-1}{\cdot}K^{-1}$
$C_{p,w}$	Specific heat of water, $J{\cdot}kg^{-1}{\cdot}K^{-1}$
$C_{p,f}$	Specific heat of air at interface temperature, $J{\cdot}kg^{-1}{\cdot}K^{-1}$
d	Half of side lengths, m
D_f	Diffusivity at the water air interface, $m^2{\cdot}s^{-1}$
h	Heat transfer coefficient, $W{\cdot}m^{-2}{\cdot}K^{-1}$
h_m	Mass transfer coefficient, $m{\cdot}s^{-1}$
k_f	Air thermal conductivity, $W{\cdot}m^{-1}{\cdot}K^{-1}$
L	Side length, m
m_s	Dried mass, kg
R	Universal gas constant = 8.314 J $kmol^{-1}{\cdot}K^{-1}$
R^2	Determination coefficient
RH_b	Relative humidity of drying medium
$RMSE$	Root-Mean-Square error
t	Time, s
T	Average temperature, K
T_b	Drying air temperature, K
Sh	Sherwood number
Nu	Nusselt number
Re	Reynolds number, $Re = (L{\cdot}v_b{\cdot}\rho_f)/\mu_f$
Sc	Schmidt number, $Sc = \mu_f/(\rho_f \cdot D_f)$
Pr	Prandtl number, $Pr = (C_{p,f} \cdot \mu_f)/k_f$
X	Average moisture content, kg/kg on dry basis
X_0	Initial moisture content, kg/kg on dry basis
X_e	Equilibrium moisture content, kg/kg on dry mass
W	Water content, % on wet basis
ρ_f	Air density at water air interface, $kg{\cdot}m^{-3}$

$\rho_{v,s}$ Vapor concentration at water air interface, kg·m^{-3}
$\rho_{v,sat}$ Saturated vapor concentration, kg·m^{-3}
$\rho_{v,b}$ Vapor concentration at drying medium, kg·m^{-3}
$\triangle E_v$ Apparent activation energy, J·mol^{-1}
$\triangle E_{v,e}$ Equilibrium activation energy, J·mol^{-1}
$\triangle H_v$ Latent heat of water vaporization, J·kg^{-1}

Appendix

A parabolic approximation of temperature inside an infinite slab can be expressed as (Chen, 2008):

$$T(x) = T_o + \left(\frac{T_s - T_o}{d^2}\right)x^2 \tag{A-1}$$

where T_o and T_s refer to the sample center and surface temperature, d is the half thickness of sample as characteristics length of slab (m), and x is the axial position (m). By taking the symmetry effect into account, the average temperature (T) of sample can be determined as follows:

$$T = \frac{\int_0^d T(x)dx}{d} \tag{A-2}$$

By combining Eqs. (A-1) and (A-2), the average temperature is found to be expressed as:

$$T = \frac{1}{3}T_s + \frac{2}{3}T_o \tag{A-3}$$

Here the surface and center temperatures can be directly determined from experimental observation.

Properties of carrot tissue (Srikiatden and Roberts, 2008; Ikegwu and Ekwu, 2009; Eim et al., 2011):

$$X_e = \left[\frac{-\ln(1-a_w)}{3.18\times10^{-4}\times(0.28+T_b)}\right]^{\frac{1}{0.95}} \tag{A-4}$$

$$C_{p,s} = 1.675 + 0.025W \tag{A-5}$$

$$C_{p,w} = 4.1762 - 9.0862\times10^{-5}T + 5.4731\times10^{-6}T^2 \tag{A-6}$$

where a_w is the water activity [the relative humidity $= \rho_{v,b}/\rho_{v,sat}\,(T_b)$], W is the moisture content (kg/kg, on wet basis), T is the product temperature (K).

References

Aoac, 1995. Official Methods of Analysis, sixteenth ed. Association of Official Analytical Chemists, Arlington, VA.

Brasiello, A., Iannone, G., Adiletta, G., De Pasquale, S., Russo, P., Matteo, M.D., 2017. Mathematical model for dehydration and shrinkage: prediction of eggplant's MRI spatial profiles. J. Food Eng. 203, 1–5.

Chen, X.D., 2008. The basics of a reaction engineering approach to modeling air-drying of small droplets or thin-layer materials. Dry. Technol. 26, 627–639.

Chen, X.D., Lin, S.X.Q., 2005. Air drying of milk droplet under constant and time-dependent conditions. AIChE J. 51, 1790–1799.

Chen, X.D., Pirini, W., Ozilgen, M., 2001. The reaction engineering approach to modelling drying of thin layer of pulped Kiwifruit flesh under conditions of small Biot numbers. Chem. Eng. Process 40, 311–320.

Chen, X.D., Xie, G.Z., 1997. Fingerprints of the drying behaviour of particulate or thin layer food materials established using a reaction engineering model. Food Bioprod. Process. 75, 213–222.

Compaore, A., Dissa, A.O., Rogaume, Y., Putranto, A., Chen, X.D., Mangindaan, D., Zoulalian, A., Remond, R., Tiendrebeogo, E.S., 2017. Application of the reaction engineering approach (REA) for modeling of the convective drying of onion. Dry. Technol. 35, 500–508.

Defraeye, T., Radu, A.I., 2018. Insights in convective drying of fruit by coupled modeling of fruit drying, deformation, quality evolution and convective exchange with the airflow. Appl. Energy 129, 1026–1038.

Eim, V.S., Rossello, C., Femenia, A., Simal, S., 2011. Moisture sorption isotherms and thermodynamic properties of carrot. Int. J. Food Eng. 7.

Fu, N., Woo, M.W., Lin, S.X.Q., Zhou, Z., Chen, X.D., 2011. Reaction engineering approach (REA) to model the drying kinetics of droplets with different initial sizes-experiments and analyses. Chem. Eng. Sci. 66, 1738–1747.

Fu, N., Woo, M.W., Selomulya, C., Chen, X.D., Patel, K., Schuck, P., Jeantet, R., 2012. Drying kinetics of skim milk with 50 wt.% initial solids. J. Food Eng. 109, 701–711.

Fu, N., Woo, M.W., Selomulya, C., Chen, X.D., 2013. Shrinkage behaviour of skim milk droplets during air drying. J. Food Eng. 116, 37–44.

Haque, M.A., Adhikari, B., Putranto, A., 2016. Predictions of drying kinetics of aqueous droplets containing WPI-lactose and WPI-trehalose by application of composite reaction engineering approach (REA). J. Food Eng. 189, 29–36.

Ikegwu, O.J., Ekwu, F.C., 2009. Thermal and physical properties of some tropical fruits and their juices in Nigeria. J. Food Technol. 7, 38–42.

Incropera, F.P., DeWitt, D.P., 1985. Fundamentals of Heat and Mass Transfer, second ed. John Wiley & Sons, NY.

Keey, R.B., 1992. Drying of loose and particulate materials. Dry. Technol. 10, 1139–1141.

Kharaghani, A., Hiep Le, K., Thi, T.H.T., Tsotsas, E., 2019. Reaction engineering approach for modeling single wood particle drying at elevated air temperature. Chem. Eng. Sci. 199, 602–612.

Kucuk, H., Midilli, A., Kilic, A., Dincer, I., 2014. A review on thin-layer drying curve equations. Dry. Technol. 32, 757–773.

Li, K., Zhang, M., Mujumdar, A.S., Chitrakar, B., 2019. Recent developments in physical field-based drying techniques for fruits and vegetables. Dry. Technol. 37, 1954–1973.

Mahiuddin, Khan, M.I.H., Kumar, C., Rahman, M.M., Karim, M.A., 2018. Shrinkage of food materials during drying: current status and challenges. Compr. Rev. Food Sci. F. 17, 1113–1126.

Mahmutoglu, T., Saygi, Y.B., Borcakli, M., Ozay, G., 1996. Effects of the pretreatment–drying method combinations on the drying rates, quality and storage stability of apricots. LWT - Food Sci. Technol. (Lebensmittel-Wissenschaft -Technol.) 29, 418–424.

Mayor, L., Sereno, A.M., 2004. Modelling shrinkage during convective drying of food materials: a review. J. Food Eng. 61, 373–386.

Mulet, A., Berna, A., Rossello, C., 1989. Drying of carrots. I. Drying models. Dry. Technol. 7, 537–557.

Mujumdar, A.S., Law, C.L., 2010. Drying technology: trends and applications in postharvest processing. Food Bioprocess Technol. 3, 843–852.

Ortizgarciacarrasco, B., Yanezmota, E., Pachecoaguirre, F.M., Ruizespinosa, H., Garciaalvarado, M.A., Corteszavaleta, O., Ruizlopez, I.I., 2015. Drying of shrinkable food products: appraisal of deformation behavior and moisture diffusivity estimation under isotropic shrinkage. J. Food Eng. 144, 138–147.

Pasternak, I.S., Gauvin, W.H., 1960. Turbulent heat and mass transfer from stationary particles. Can. J. Chem. Eng. 38, 35–42.
Patel, K.C., Chen, X.D., Lin, S.X.Q., Adhikari, B., 2009. A composite reaction engineering approach to drying of aqueous droplets containing sucrose, maltodextrin (DE6) and their mixtures. AIChE J. 55, 217–231.
Putranto, A., Chen, X.D., 2013. Spatial reaction engineering approach as an alternative for nonequilibrium multiphase mass-transfer model for drying of food and biological materials. AIChE J. 59, 55–67.
Putranto, A., Chen, X.D., 2014. A simple and effective model for modeling of convective drying of sewage sludge: the reaction engineering approach (REA). Procedia Chem. 9, 77–87.
Putranto, A., Chen, X.D., 2016a. Microwave drying at various conditions modeled using the reaction engineering approach. Dry. Technol. 34, 1654–1663.
Putranto, A., Chen, X.D., 2016b. The relative activation energy of food materials: important parameters to describe drying kinetics. Int. J. Food Prop. 19, 1726–1737.
Putranto, A., Chen, X.D., Webley, P.A., 2011. Modeling of drying of food materials with thickness of several centimeters by the reaction engineering approach (REA). Dry. Technol. 29, 961–973.
Ranz, W.E., Marshall, W.R.J., 1952. Evaporation from drops: part 1. Chem. Eng. Prog. 48, 141–146.
Saha, B., Bucknall, M.P., Arcot, J., Driscoll, R.H., 2018. Derivation of two layer drying model with shrinkage and analysis of volatile depletion during drying of banana. J. Food Eng. 226, 42–52.
Sander, A., Kardum, J.P., Skansi, D., 2001. Transport properties in drying of solids. Chem. Biochem. Eng. Q. 15, 131–137.
Singh, P., Talukdar, P., 2019. Determination of shrinkage characteristics of cylindrical potato during convective drying using novel image processing technique. Heat Mass Tran. 1–13.
Srikiatden, J., Roberts, J.S., 2008. Predicting moisture profiles in potato and carrot during convective hot air drying using isothermally measured effective diffusivity. J. Food Eng. 84, 516–525.
Suzuki, K., Ihara, K., Kubota, K., Hosaka, H., 1977. Heat transfer coefficient of the constant rate period in the drying of agar gel, carrot and sweet potato. J. Food Sci. Tech. Mys. 24, 387–393.